We believe that the present study represents a significant step beyond the observation of long-range order loss that was made in previous X-ray experiments on ultrafast non-thermal melting: in these previous experiments, it was not possible to obtain the initial displacements. Although the relationship between the large coherent displacements of the lattice atoms observed in the present work and the stability of the parent phase is still elusive, our experiments establish a direction for future studies—the use of X-ray scattering on the appropriate timescale to reveal details of product phase formation. □

Methods

The X-ray pulses were generated by focusing femtosecond laser pulses from a titanium:sapphire laser system (120-fs pulse width, about 100-mJ pulse energy, 10-Hz repetition rate) onto a thin titanium wire to produce a microplasma[21]. The incoherent X-ray emission from the laser-produced plasma (Ti K_α line at 0.274 nm) was collected, and focused onto a spot of approximately 80 μm in the centre of the laser-excited area on the surface of the bismuth crystal. To focus the X-rays, we used a toroidally bent silicon crystal. The 50-nm Bi films were grown heteroepitaxially on a Si(111) wafer. The growth process provided high-quality single crystalline layers of bismuth with a lattice constant different from that of the Si substrate. This allows us to isolate the relatively weak X-ray diffraction of the thin Bi film from the strong background diffraction due to the Si substrate. An X-ray-sensitive electronic camera was used to record the angular distribution of the diffracted X-rays. The X-ray signal integrated over the diffraction angle (integrated reflectivity) typically corresponded to 10 diffracted photons per pulse. Therefore, signal integration over many thousands of pulses was necessary to achieve a measuring accuracy of several per cent.

Received 7 October 2002; accepted 7 February 2003; doi:10.1038/nature01490.

1. Bloembergen, N. From nanosecond to femtosecond science. *Rev. Mod. Phys.* **71,** S283–S287 (1999).
2. Chin, A. H. *et al.* Ultrafast structural dynamics in InSb probed by time-resolved X-ray diffraction. *Phys. Rev. Lett.* **83,** 336–339 (1999).
3. Siders, C. W. *et al.* Detection of non-thermal melting by ultrafast X-ray diffraction. *Science* **286,** 1340–1342 (1999).
4. Lindenberg, A. M. *et al.* Time-resolved X-ray diffraction from coherent phonons during a laser-induced phase transition. *Phys. Rev. Lett.* **84,** 111–114 (2000).
5. Rousse, A. *et al.* Non-thermal melting in semiconductors measured at femtosecond resolution. *Nature* **410,** 65–68 (2001).
6. Sokolowski-Tinten, K. *et al.* Femtosecond X-ray measurement of ultrafast melting and large acoustic transients. *Phys. Rev. Lett.* **87,** 225701 (2001).
7. Cavalleri, A. *et al.* Femtosecond structural dynamics in VO_2 during an ultrafast solid-solid phase transition. *Phys. Rev. Lett.* **87,** 237401 (2001).
8. Feurer, T. *et al.* Femtosecond silicon K_α pulses from laser produced plasmas. *Phys. Rev. E* **65,** 016412 (2002).
9. Lindemann, F. A. Über die Berechnung molekularer Eigenfrequenzen. *Phys. Z.* **11,** 609–612 (1910).
10. Born, M. Thermodynamics of crystals and melting. *J. Chem. Phys.* **7,** 591–603 (1939).
11. Tallon, J. L. A hierarchy of catastrophes as a succession of stability limits for the crystalline state. *Nature* **342,** 658–660 (1989).
12. Madelung, O. (ed.) *Semiconductors: Physics of Non-tetrahedrally Bonded Elements and Binary Compounds I* in Landolt-Börnstein, New Series, Group III: *Crystal and Solid State Physics* Vol. 17, *Semiconductors*, Part a (Springer, Berlin, 1983).
13. Peierls, R. *More Surprises in Theoretical Physics* (Princeton Univ. Press, Princeton, 1991).
14. Shick, A. B., Ketterson, J. B., Novikov, D. L. & Freeman, A. J. Electronic structure, phase stability, and semimetal-semiconductor transitions in Bi. *Phys. Rev. B* **60,** 15484–15487 (1999).
15. Zeiger, H. J. *et al.* Theory for displacive excitation of coherent phonons. *Phys. Rev. B* **45,** 768–778 (1992).
16. Hunsche, S., Wienecke, K., Dekorsy, T. & Kurz, H. Impulsive softening of coherent phonons in tellurium. *Phys. Rev. Lett.* **75,** 1815–1818 (1995).
17. Garrett, G. A., Albrecht, T. F., Whitaker, J. F. & Merlin, R. Coherent THz phonons driven by light pulses and the Sb problem: what is the mechanism? *Phys. Rev. Lett.* **77,** 3661–3664 (1996).
18. Hase, M., Mizoguchi, K., Harima, H. & Nakashima, S. Dynamics of coherent phonons in bismuth generated by ultrashort light pulses. *Phys. Rev. B* **58,** 5448–5452 (1998).
19. DeCamp, M. F., Reis, D. A., Bucksbaum, P. H. & Merlin, R. Dynamics and coherent control of high-amplitude phonons in bismuth. *Phys. Rev. B* **64,** 092301 (2001).
20. Hase, M., Kitajima, M., Nakashima, S. & Mizoguchi, K. Dynamics of coherent anharmonic phonons in bismuth using high density photoexcitation. *Phys. Rev. Lett.* **88,** 067401 (2002).
21. Von der Linde, D. *et al.* 'Ultrafast' extended to X-rays: Femtosecond time-resolved X-ray diffraction. *Z. Phys. Chem.* **215,** 1527–1541 (2001).

Acknowledgements Financial support by the Deutsche Forschungsgemeinschaft, the European Community (Research and Training Network XPOSE) and the German Academic Exchange Service (DAAD) is acknowledged.

Competing interests statement The authors declare that they have no competing financial interests.

Correspondence and requests for materials should be addressed to K.S.-T. (e-mail: kst@ilp.physik.uni-essen.de).

Phonon interpretation of the 'boson peak' in supercooled liquids

T. S. Grigera*†, V. Martín-Mayor*†, G. Parisi* & P. Verrocchio†‡

** Dipartimento di Fisica, Sezione INFN, SMC and INFM unità di Roma 1, Università di Roma "La Sapienza", Piazzale Aldo Moro 2, I-00185 Roma, Italy*
‡ Dipartimento di Fisica and INFM unità di Trento, Università di Trento, Via Sommarive, 14, 38050 Povo, Trento, Italy

Glasses[1,2] are amorphous solids, in the sense that they display elastic behaviour. In crystalline solids, elasticity is associated with phonons, which are quantized vibrational excitations. Phonon-like excitations also exist in glasses at very high (terahertz; 10^{12} Hz) frequencies; surprisingly, these persist in the supercooled liquids[3]. A universal feature of such amorphous systems is the boson peak: the vibrational density of states has an excess compared to the Debye squared-frequency law. Here we investigate the origin of this feature by studying the spectra of inherent structures[4] (local minima of the potential energy) in a realistic glass model. We claim that the peak is the signature of a phase transition in the space of the stationary points of the energy, from a minima-dominated phase (with phonons) at low energy to a saddle-point-dominated phase[5–7] (without phonons). The boson peak moves to lower frequencies on approaching the phonon–saddle transition, and its height diverges at the critical point. Our numerical results agree with the predictions of euclidean random matrix theory[8] on the existence of a sharp phase transition[9] between an amorphous elastic phase and a phonon-free one.

Vibrational excitations of glasses in the terahertz region, and the related vibrational density of states (VDOS), are important in their thermodynamic properties[10]. Recent results suggest that the VDOS is determined by the properties of the potential energy landscape[4] (PEL), a tool useful in the understanding of the slow dynamics of supercooled liquids[2]. Indeed, the VDOS and the dynamic structure factor can be qualitatively reproduced from the (harmonic) vibrational spectrum obtained from the diagonalization of the hessian matrix of the potential energy evaluated at the minima ('inherent structures') of a Lennard–Jones system[11]. The same numerical procedure has led to quantitative agreement with inelastic X-ray scattering experiments in amorphous silica[12]. Here we will show that a boson peak must be present in the VDOS as a consequence of the PEL geometry; we also make quantitative predictions, which can be checked by rapidly quenching supercooled liquids below their glass temperature.

The high-frequency (0.1–10 THz) excitations have been experimentally shown to have linear dispersion relations[3,13–18] in the mesoscopic momentum region ($\sim$1–10 nm^{-1}). Although clearly not plane waves, they are highly reminiscent of phonons, both because they propagate with the speed of sound, and because the VDOS $g(\omega)$ (ω is the frequency) is Debye-like ($g(\omega) \propto \omega^2$) at low enough frequency. These excitations have in fact been dubbed 'high-frequency sound', and a coherent theoretical picture of their properties has been obtained[9,19,20] using euclidean random matrix theory[8] (ERMT).

However, there is more to the low-frequency VDOS of glasses than the Debye law. A characteristic feature is that the VDOS departs from the Debye form, displaying an excess of states, which has been named the boson peak. As observed in many materials[3,13–18], the boson peak is in a region of frequencies where

† Present addresses: Centro di Studi e Ricerche "Enrico Fermi", via Panisperna, 89/A, 00184 Roma, Italy (T.S.G.); Departamento de Física Teórica I, Universidad Complutense de Madrid, Avenida Complutense, 28040 Madrid, Spain (V.M.-M., P.V.).

the dispersion relation for phonons is still linear (ω is a few terahertz). Several non-equivalent ways of experimentally defining the boson peak have been introduced. One approach defines it as a peak in Raman scattering data, another as a peak in the difference between the VDOS of the glass and the corresponding crystal. Other authors extract $g(\omega)$ from their neutron scattering data and look for a peak in $g(\omega)/\omega^2$. This is the definition that we adopt, because we believe that it reveals universal properties of glasses.

The origin of the boson peak can be understood if we consider the ensemble of generalized inherent structures (GISs): for each equilibrium configuration, the associated GIS is the nearest stationary point of the hamiltonian. If we start from an equilibrium configuration at low temperature, the GIS is a local minimum, and it coincides with the more frequently used inherent structure (that is, the nearest minimum of the hamiltonian). On the contrary, if we start from high temperature, the GISs are saddle points. In the GIS ensemble there is a sharp phase transition separating these two regimes. It takes place in glass-forming liquids[5–7] at the mode-coupling temperature[21,22] (T_{MC}), above which liquid diffusion is no longer ruled by rare 'activated' jumps between inherent structures, but by motion along the unstable directions of saddles. Phonons are present in the spectrum of the VDOS in the low-temperature phase (inherent-structure dominated), but are absent in the saddle phase (see ref. 23 for a different approach).

The key point, following both from analytic computations in soluble models[24] and simulations[5–7], is that the minima obtained starting from configurations below T_{MC} and the saddles obtained starting above T_{MC} join smoothly at T_{MC}. Thus we can study GISs as a single ensemble, parameterized by the initial temperature or the final energy. We expect that the GIS ensemble belongs to a large universality class.

This transition from the phonon phase to the saddle phase is a general phenomenon that is not restricted to glasses. It has been studied in the framework of ERMT[8], showing[9] that close to this transition, a boson peak is present in the phonon phase, whose position shifts to lower frequencies on approaching the transition point, while its height grows without bound. The boson peak actually signals a crossover at frequency ω_{BP} between a (phonon dominated) ω^2 scaling of $g(\omega)$ to an ω^γ scaling ($\gamma < 2$) that is present at the phase transition point. More precisely, at frequencies that are small with respect to the Debye frequency, the VDOS should satisfy the scaling law

$$g(\omega, \Delta) = \omega^\gamma h(\omega \Delta^{-\rho}) \quad (1)$$

where Δ is the distance from the critical point and depends on the actual control parameter (pressure, temperature, and so on) and $h(x)$ is such that $h(x) \propto x^{2-\gamma}$ for $x \ll 1$ and $h(x)$ is approximately equal to a constant for $x \gg 1$. This scaling law implies that

$$\omega_{BP} \propto \Delta^\rho, \quad g(\omega_{BP})/\omega_{BP}^2 \propto \Delta^{-\beta} \quad (2)$$

where $\beta = \rho(2-\gamma)$. Under the resummation of a given class of diagrams, ERMT predicts[9] that $\rho = 1$, $\gamma = 3/2$ and $\beta = 1/2$. The actual (universal) values of these critical exponents in three dimensions may differ slightly from the values found in this approximation.

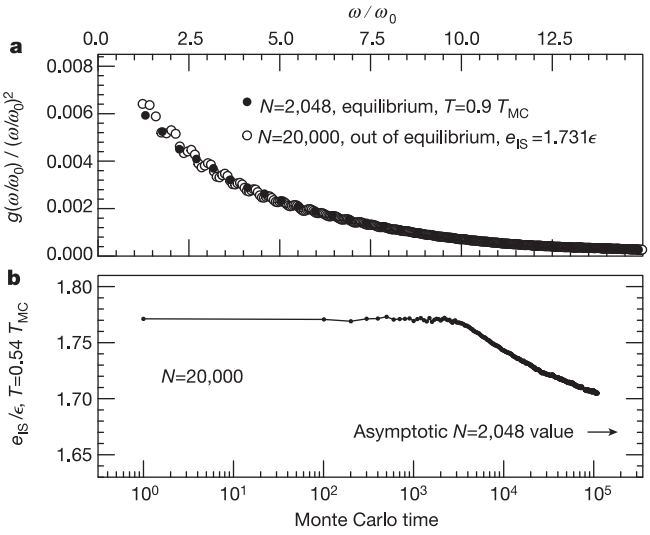

Figure 1 The vibrational density of states, $g(\omega)$, at low frequencies depends only on the energy of the inherent structure, e_{IS}. **a**, $g(\omega/\omega_0)/(\omega/\omega_0)^2$ (where ω_0 is the unit of frequency defined below) for an equilibrated 2,048-particle system at $T = 0.9T_{MC}$ compared to that obtained from ten inherent structures of the same e_{IS} from a 20,000-particle system out of equilibrium. The larger system was quenched from infinite temperature to $T = 0.54T_{MC}$, and the inherent structures obtained by minimizing instantaneous configurations between 1.9×10^4 and 2×10^4 Swap Monte Carlo steps. Similar results are obtained at all the temperatures for which comparable e_{IS} are obtained in the quench. Inherent structures were found by minimizing instantaneous configurations with a conjugate gradient algorithm. The hessian was diagonalized with standard library routines in the case of the smaller system, and with the method of moments for the larger system. Each VDOS was obtained from at least 200 inherent structure as the histogram of the square root of the eigenvalues. **b**, Monte Carlo history of e_{IS} on a logarithmic timescale, for the system of 20,000 particles suddenly quenched from infinite temperature to $T = 0.54T_{MC}$. The soft-sphere binary mixture is made of 50% of particles of type A and 50% of type B, both with the same mass. The interaction potential is $V_{\alpha\beta}(r) = \varepsilon[(\sigma_\alpha + \sigma_\beta)/r]^{12} + C_{\alpha\beta}(\alpha, \beta \in \{A, B\})$, with σ values fixed by the conditions $\sigma_B = 1.2\sigma_A$, and $(2\sigma_A)^3 + 2(\sigma_A + \sigma_B)^3 + (2\sigma_B)^3 = 4\sigma_0$. A smooth cut-off is imposed at $r_c = \sqrt{3}\sigma_0$: for $r_c \le r \le a$, we set $V_{\alpha\beta} = B_{\alpha\beta}(a-r)^3$, and $V_{\alpha\beta} = 0$ for $r > a$. In the results, lengths are given in units of σ_0, energies in units of ε, and frequencies in units of $\omega_0 \equiv (m\sigma_0^2/\varepsilon)^{-1/2}$. Using argon parameters ($\sigma_0 = 3.4$ Å, $\varepsilon = 120$ K k_B (k_B is Boltzmann's constant), and $m = 39.96$ a.m.u.), the frequency unit ω_0 is 0.46 THz and the mode coupling temperature T_{MC} is 26.4 K. All runs are at constant volume, with particle density $\rho = \sigma_0^{-3}$. For temperatures down to $T = 0.9T_{MC}$ thermalization was achieved, as checked by ensuring that the equilibrium fluctuation–dissipation ratio is reached. For $T < 0.9T_{MC}$, the runs were followed until e_{IS} reached stationarity.

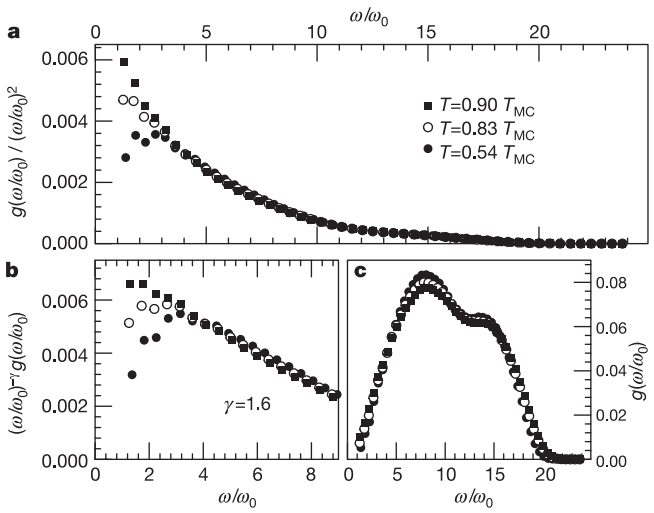

Figure 2 The vibrational density of states $g(\omega)$ of the soft-sphere binary mixture at three representative temperatures. (The full set of temperatures was $T/T_{MC} = 0.9$, 0.83, 0.78, 0.69, 0.61, 0.54 and 0.49; frequencies are given in units of ω_0). **a**, The $g(\omega)/\omega^2$ plot shows a boson peak at low temperature (shown for $T = 0.54T_{MC}$). When temperature is increased, the peak shifts to lower frequencies and grows without bound. **b**, The divergence seen in **a** is due to an ω^γ (with $\gamma < 2$) scaling of $g(\omega)$. At temperatures where the boson peak is still seen, a crossover between ω^2 and ω^γ scaling is noted (compare **a** and **b)**. Although γ cannot be extracted very accurately from the data, it is compatible with $\gamma = 2 - \beta/\rho \approx 1.6$, with β and ρ taken from the fits of Fig. 3. **c**, The high-frequency features of $g(\omega)$ do not change drastically with temperature.

We now analyse numerically the existence of such a transition by studying the soft-sphere binary mixture, a model of a fragile glass[25]. We simulate this system with the Swap Monte Carlo algorithm[26], and compute the VDOS of the inherent structures obtained starting from equilibrium configurations at temperatures below T_{MC}. Except where stated, we used 2,048 particles, and runs were followed until the energy of the inherent structure, e_{IS}, reached a stationary value. The predictions above agree with the numerical data, taking $\Delta = e_c - e_{IS}$ (where e_c is the critical value of e_{IS}).

Given the numerical results of ref. 27, we expect that $g(\omega)$ will depend only on e_{IS}, and thus that e_{IS} is the relevant control parameter. To check this, we compare the VDOS of two systems at different temperatures (one in equilibrium, the other not) but with the same e_{IS}. The equilibrated system has 2,048 particles, whereas the other has 20,000 and is in the regime where e_{IS} has not yet stabilized after a quench (Fig. 1b). As Fig. 1a shows for a representative case, the VDOS obtained at the same e_{IS} for the two systems coincides, confirming that e_{IS} is indeed the control parameter. We can thus proceed to investigate the scaling laws, shown in equation (2).

The VDOS at three representative temperatures is shown in Fig. 2. For temperatures up to $T = 0.69T_{MC}$, a Debye behaviour ($g(\omega) \propto \omega^2$) is found for the lowest frequencies that can be resolved in a system of this size. In the $g(\omega)/\omega^2$ plot (Fig. 2a), a peak is clearly identified, which is seen to grow in height and shift to lower frequency on raising the temperature. The peak shifts to frequencies below our resolution for $T > 0.69T_{MC}$, but we can identify a Debye region up to $T = 0.83T_{MC}$. Above this temperature the Debye region is not well defined, and it disappears completely for $T \geq 0.9T_{MC}$. At these temperatures, $g(\omega)/\omega^2$ seems to diverge (at least within the frequency range that we can resolve). Experimentally, this behaviour may be difficult to observe owing to the presence of the elastic peak, but B_2O_3 data[28] seem to support this prediction. For frequencies immediately above ω_{BP}, the VDOS scales as ω^γ, with $\gamma \approx 1.5$ (Fig. 2b). Note that these changes of the VDOS with temperature go practically unnoticed if one plots $g(\omega)$ directly (Fig. 2c). In particular, the boson peak is completely unrelated to the first maximum of $g(\omega)$, whose position is insensitive to temperature changes.

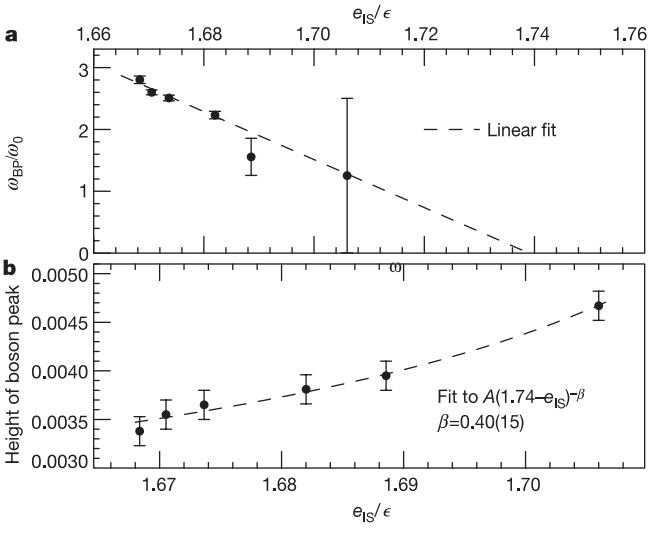

Figure 3 Scaling of the position and height of the boson peak near the liquid–phonon transition. (Energies and frequencies are in units of ε and ω_0, respectively.) **a**, The position of the boson peak, ω_{BP}, is linear in the control parameter, in this case the energy of the inherent structures e_{IS}. Extrapolating with a linear fit, ω_{BP} goes to 0 at $e_{IS} = e_c = 1.74(1)\varepsilon$. **b**, The height of the boson peak diverges as a power law (the leftmost point has been left out of the fit). The height and position of the boson peak were obtained by fitting a parabola to the peak of $g(\omega)/\omega^2$ at $T/T_{MC} = 0.49$, 0.54, 0.61, 0.69, 0.78 and 0.83. The corresponding e_{IS}/ε are 1.668, 1.671, 1.674, 1.682, 1.689 and 1.707.

Because we know that e_{IS} decreases slowly with time after a quench[27] (see also Fig. 1b), the above results enable us to make predictions about the ageing of the VDOS, and in particular of the boson peak. With increasing time the system moves farther from the critical point, and thus the boson peak should decrease in height and shift to higher frequencies. Moreover, at a given frequency (below the asymptotic ω_{BP}) $g(\omega)$ should decrease, as it will be of the order of ω^γ at short times and of the order of ω^2 at very long times. Similarly, we expect a cooling-rate dependence of the shape of the boson peak: the slower the cooling, the lower the asymptotic e_{IS}, and thus the larger the ω_{BP} and the less pronounced the boson peak. An effect of this kind has been observed in As_3S_3 (ref. 29), although in that work it is difficult to disentangle the physical effect from the chemical changes of the sample due to dissociation. To our knowledge, a clear-cut experimental observation of these effects has not been reported.

Using all the spectra for which the peak position can be clearly identified, we find that the relationship between ω_{BP} and the energy of the inherent structure is linear (Fig. 3a). The energy at which ω_{BP} becomes zero, e_c, is found from a linear fit as $e_c = 1.74\varepsilon$ (ε is the energy scale). As for the height of the peak, the points up to $T = 0.83T_{MC}$ are compatible with a power-law divergence of the form shown in equation (2) (Fig. 3b). Fixing e_c at the value 1.74ε arising from the linear fit of ω_{BP} versus e_{IS}, a power-law fit yields an exponent $\beta = 0.040 \pm 0.15$; if the exponent is fixed at $\beta = 1/2$, then the critical value is obtained as $e_c = 1.752 \pm 0.002\varepsilon$. Thus the numerical data are compatible with the theoretically predicted scaling, although we have not been able to work close to the critical point, and thus cannot attain great accuracy in the critical exponents or the critical point.

The present discussion applies to experiments as long as the system is in the regime where the inverse frequency is much larger than the structural relaxation time, when the harmonic approximation is applicable[30]. Thus, although the boson peak observed in liquids can be understood by the present considerations, one should not expect to actually arrive close to the critical point in equilibrium measurements. Rather, one should generate a glass by hyperquenching (see, for example, http://www.df.unipi.it/workshop/oral/OL6.pdf): for such a system, we predict that the boson peak measured at low temperature should obey the scaling of equation (2), the control parameter being the fictive temperature (that is, the temperature at which the value of e_{IS} actually reached would be the equilibrium value). In our instantaneous quench, the fictive temperature is simply the temperature at which the hyperquench starts; but in experiments, the cooling rate will also have an effect. In this way, the problem of swamping by the quasielastic peak should also be alleviated.

The significance of the value $e_c = 1.74(1)\varepsilon$ is twofold. First, it is the value of e_{IS} that corresponds, in equilibrium, to $T = T_{MC}$, the mode-coupling critical temperature (which we have independently determined as in ref. 22, using a standard Metropolis Monte Carlo without swap moves). Second, it coincides within errors with the threshold energy below which the ratio of the number of saddle points to the number of minima vanishes exponentially with the number of particles[7] (our numerical accuracy on e_c is similar to that of ref. 7). Thus we find a link between the onset of slow dynamics, the appearance of phonon-like excitations, and a geometrical phase transition of the PEL in fragile glasses. At variance with previous PEL studies, the clear link between the PEL geometrical transition and high-frequency dynamics allows it to be studied experimentally by following the evolution of the boson peak.

We have studied numerically the VDOS of a fragile glass-former undergoing its mode-coupling transition. We have found that in the ensemble of the stationary points near the equilibrium configurations (GISs) there is a transition from a mechanically unstable phase where saddles are present to a stable phase where phonon-like

excitations appear. The scaling laws predicted by ERMT are compatible with the numerical results that we have obtained for the soft-sphere model. This approach is equivalent to other microscopic descriptions of the glass transition based on the geometry of the PEL[5–7,31]. But this point of view emphasizes quantities accessible to experiment, like the VDOS, and proposes an interpretation of a universal feature of glasses, the boson peak. This peak appears in the phonon phase, and it is a signature of a cross-over from a phonon-dominated spectrum with a Debye ω^2 scaling to an ω^γ, $\gamma \approx 1.5$ spectrum, resulting from the hybridization of acoustic modes with high-energy modes that soften upon approaching the saddle–phonon transition[9]. The ERMT predictions (equations (1) and (2)) could be checked experimentally in hyperquenching experiments, where the boson peak should strongly depend on the fictive temperature. We expect that the 'saddle–phonon transition' point of view will be able to bridge the realms of experiment and numerical studies of the PEL, allowing the testing of many geometrical ideas, and the use of insights derived from PEL in the detailed analysis of the experimental glass transition. □

Received 10 July 2002; accepted 30 January 2003; doi:10.1038/nature01475.

1. Angell, C. A. Formation of glasses from liquids and biopolymers. *Science* **267,** 1924–1935 (1995).
2. DeBenedetti, P. G. & Stillinger, F. H. Supercooled liquids and the glass transition. *Nature* **410,** 259–267 (2001).
3. Sette, F., Krisch, M. H., Masciovecchio, C., Ruocco, G. & Monaco, G. Dynamics of glasses and glass-forming liquids studied by inelastic X-ray scattering. *Science* **280,** 1550–1555 (1998).
4. Stillinger, F. H. A topographic view of supercooled liquids and glass formation. *Science* **267,** 1935–1939 (1995).
5. Angelani, L., Di Leonardo, R., Ruocco, G., Scala, A. & Sciortino, F. Saddles in the energy landscape probed by supercooled liquids. *Phys. Rev. Lett.* **85,** 5356–5359 (2000).
6. Broderix, K., Bhattacharya, K. K., Cavagna, A., Zippelius, A. & Giardina, I. Energy landscape of a Lennard-Jones liquid: Statistics of stationary points. *Phys. Rev. Lett.* **85,** 5360–5363 (2000).
7. Grigera, T. S., Cavagna, A., Giardina, I. & Parisi, G. Geometric approach to the dynamic glass transition. *Phys. Rev. Lett.* **88,** 055502 (2002).
8. Mézard, M., Parisi, G. & Zee, A. Spectra of euclidean random matrices. *Nucl. Phys. B* **559,** 689–701 (1999).
9. Grigera, T. S., Martín-Mayor, V., Parisi, G. & Verrocchio, P. Vibrations in glasses and Euclidean random matrix theory. *J. Phys. Condens. Matter* **14,** 2167–2179 (2002).
10. Phillips, W. A., Buchenau, U., Nücher, N., Dianoux, A.-J. & Petry, W. Dynamics of glassy and liquid selenium. *Phys. Rev. Lett.* **63,** 2381–2384 (1989).
11. Ruocco, G. *et al.* Relaxation processes in harmonic glasses? *Phys. Rev. Lett.* **84,** 5788–5791 (2000).
12. Pilla, O. *et al.* Transverse acoustic nature of the excess of vibrational states in vitreous silica. Preprint cond-mat/0209519 at ⟨http://xxx.lanl.gov⟩ (2002).
13. Masciovecchio, C. *et al.* Observation of large-momentum phononlike modes in glasses. *Phys. Rev. Lett.* **76,** 3356–3359 (1996).
14. Matic, A. *et al.* Contrasting behaviour of acoustic modes in network and non-network glasses. *Europhys. Lett.* **54,** 77–83 (2001).
15. Masciovecchio, C. *et al.* High-frequency propagating modes in vitreous silica at 295 K. *Phys. Rev. B* **55,** 8049–8051 (1997).
16. Benassi, P. *et al.* Evidence of high frequency propagating modes in vitreous silica. *Phys. Rev. Lett.* **77,** 3835–3838 (1996).
17. Fioretto, D. *et al.* High-frequency dynamics of glass-forming polybutadiene. *Phys. Rev. E* **59,** 4470–4475 (1999).
18. Pilla, O. *et al.* Nature of the short wavelength excitations in vitreous silica: An X-ray Brillouin scattering study. *Phys. Rev. Lett.* **85,** 2136–2139 (2000).
19. Martín-Mayor, V., Mézard, M., Parisi, G. & Verrocchio, P. The dynamical structure factor in topologically disordered systems. *J. Chem. Phys.* **114,** 8068–8081 (2001).
20. Grigera, T. S., Martín-Mayor, V., Parisi, G. & Verrocchio, P. Vibrational spectrum of topologically disordered systems. *Phys. Rev. Lett.* **87,** 085502 (2001).
21. Götze, W. & Sjorgen, L. Relaxation processes in supercooled liquids. *Rep. Prog. Phys.* **55,** 241–376 (1992).
22. Kob, W. & Andersen, H. C. Testing mode-coupling theory for a supercooled binary Lennard-Jones mixture I: The van Hove correlation function. *Phys. Rev. E* **51,** 4626–6241 (1995).
23. Göetze, W. & Mayr, M. Evolution of vibrational excitations in glassy systems. *Phys. Rev. E* **61,** 587–606 (2000).
24. Cavagna, A., Giardina, I. & Parisi, G. Role of saddles in mean-field dynamics above the glass transition. *J. Phys. A* **34,** 5317–5326 (2001).
25. Bernu, B., Hansen, J.-P., Hiwatari, Y. & Pastore, G. Soft-sphere model for the glass transition in binary alloys: Pair structure and self-diffusion. *Phys. Rev. A* **36,** 4891–4903 (1987).
26. Grigera, T. S. & Parisi, G. Fast Monte Carlo algorithm for supercooled soft spheres. *Phys. Rev. E* **63,** 045102 (2001).
27. Kob, W., Sciortino, F. & Tartaglia, P. Aging as dynamics in configuration space. *Europhys. Lett.* **49,** 590–596 (2000).
28. Engberg, D. *et al.* Origin of the boson peak in a network glass B_2O_3. *Phys. Rev. B* **59,** 4053–4057 (1999).
29. Mamedov, S., Kisliuk, A. & Quitmann, D. Effect of preparation conditions on the low frequency Raman spectrum of glassy As_2S_3. *J. Mater. Sci.* **33,** 41–43 (1998).
30. Horbach, J., Kob, W. & Binder, K. The specific heat of amorphous silica within the harmonic approximation. *J. Phys. Chem. B* **103,** 4104–4108 (1999).
31. La Nave, E., Stanley, H. E. & Sciortino, F. Configuration space connectivity across the fragile-to-strong transition in silica. *Phys. Rev. Lett.* **88,** 035501 (2002).

Acknowledgements We thank O. Pilla, G. Ruocco and G. Viliani for discussions. We are grateful to the RTN3 collaboration for CPU time in their cluster. V.M.M. was supported in part by the European Commission and the Spanish OCYT.

Competing interests statement The authors declare that they have no competing financial interests.

Correspondence and requests for materials should be addressed to V.M.-M. (e-mail: victor.martin@roma1.infn.it).

Detection of human influence on sea-level pressure

Nathan P. Gillett*, Francis W. Zwiers†, Andrew J. Weaver* & Peter A. Stott‡

** School of Earth and Ocean Sciences, University of Victoria, PO Box 3055, Victoria, British Columbia, V8W 3P6, Canada*
† Canadian Centre for Climate Modelling and Analysis, Meteorological Service of Canada, PO Box 1700, STN CSC, Victoria, British Columbia, V8W 2Y2, Canada
‡ Hadley Centre for Climate Prediction and Research, Met Office, Bracknell, Berkshire RG12 2SY, UK

Greenhouse gases and tropospheric sulphate aerosols—the main human influences on climate—have been shown to have had a detectable effect on surface air temperature[1–3], the temperature of the free troposphere and stratosphere[2,4] and ocean temperature[5,6]. Nevertheless, the question remains as to whether human influence is detectable in any variable other than temperature. Here we detect an influence of anthropogenic greenhouse gases and sulphate aerosols in observations of winter sea-level pressure (December to February), using combined simulations from four climate models. We find increases in sea-level pressure over the subtropical North Atlantic Ocean, southern Europe and North Africa, and decreases in the polar regions and the North Pacific Ocean, in response to human influence. Our analysis also indicates that the climate models substantially underestimate the magnitude of the sea-level pressure response. This discrepancy suggests that the upward trend in the North Atlantic Oscillation index[7] (corresponding to strengthened westerlies in the North Atlantic region), as simulated in a number of global warming scenarios[8–10], may be too small, leading to an underestimation of the impacts of anthropogenic climate change on European climate.

We use gridded observations of decadal mean December–February sea-level pressure (1948–1998) taken from three sources: a version of the HadSLP data set derived using only surface observations[11], the National Centers for Environmental Prediction (NCEP) reanalysis[12], and an updated version of the Trenberth data set[13]. Intercomparison of these data sets indicates that agreement is generally good over those regions covered by observations, and that the Trenberth data and NCEP reanalysis differ mainly over Greenland and the Himalayas, probably owing to differences in the reduction of surface pressure to sea level. In regions where there are few surface observations, such as the Antarctic, the NCEP reanalysis is likely to be less reliable than in the better-sampled regions covered by all three data sets. We use ensembles of integrations with historical greenhouse gas and sulphate aerosol forcing from four coupled ocean–atmosphere climate models: the first and second Canadian Centre for Climate Modelling and Analysis coupled models, CGCM1 and CGCM2, and the second and third Hadley Centre coupled models, HadCM2 and HadCM3.

Figure 1 shows the trend in sea-level pressure over the 1948–1998 period in the NCEP reanalysis (Fig. 1a) and the multi-model mean

